Propagation effects in two-color coherent-control processes

Ce Chen and D. S. Elliott
School of Electrical Engineering, Purdue University, West Lafayette, Indiana 47907
(Received 21 August 1995)

We have investigated a two-color coherent-control process at high densities of the absorbing medium. Irradiating a vapor of atomic mercury with a coherent field, with one component nearly resonant with the three-photon $6s\ ^1S_0 \rightarrow 6p\ ^1P_1^o$ transition, and the other component the third harmonic of the first, we observe the interference between the two excitation pathways for this transition. Measurements of this interaction as the density of the mercury vapor is increased show evidence of nonlinear coupling (phase and amplitude locking) of the two field components with each other. This is manifested as a decrease in the magnitude of the photoionization signal, as well as a decrease of the depth of modulation of the photoionization signal.

PACS number(s): 32.80.Qk

I. INTRODUCTION

The coherent control of optical processes through the manipulation of the relative phase and amplitude of interfering transition amplitudes has been investigated by many groups in recent years. The prospect for using these processes to control the quantum yield of optical interactions has motivated much of this work [1]. Interference in the production of a single product is observable when two coherent pathways from one initial state to one final state are driven concurrently. The net transition rate depends on the relative amplitude and phase of the optical field components driving the interactions, and variation of the phase difference between the field components can result in a change from strong enhancement (constructive interference) of a process to complete inhibition (destructive interference). Coherent control becomes more interesting when more than one final state is accessed by the laser field, since then it is possible to control branching ratios between product states.

This interference has been exploited in several observations. When applied to a bound-bound transition, modulation of resonantly enhanced multiphoton ionization of atomic mercury [2] and of molecular HCl [3] has been observed. When applied to a bound-free transition, phase-dependent photoelectron angular distributions in atomic [4–6] and molecular [7] systems, as well as modulation of the ionization probability [8], have been observed. DiMauro *et al.* [9] have been able to control the angular distribution of photofragments in the photodissociation of HD^+. Directional photoejection has also been observed in solid-phase materials, including the cathode of a photomultiplier [10], bulk glass media [11], and a GaAs quantum well structure [12]. More recently, Gordon, *et al.* [13] have reported successful control over the branching ratio of photodissociation product states of HI for certain wavelength ranges of the photodissociating laser. While the processes for this last demonstration have not yet been elucidated, this work bodes well for future applications of coherent control processes in complex molecular systems. Nakajima and Lambropoulos [14] have shown theoretically that the Fano profile of an autoionizing resonance can be strongly controlled through this interference as well.

In this paper we present results from our experimental studies of interference in dense absorbing media. It is desirable to apply coherent control techniques to media of as high a density as possible in order to maximize yields. It is already clearly established that in many cases the density cannot be increased without bound, as locally generated fields have been shown to suppress resonantly enhanced multiphoton ionization processes at high pressures in a variety of examples [15–18]. These effects were predicted as early as the mid-1960s by Manykin and Afanas'ev [19] and Gurevich and Khronopulo [20], who studied parametric effects in three-wave mixing and two-photon resonantly enhanced third-harmonic generation. Several additional experimental [21–24] and theoretical investigations [25–29] played an important role in the interpretation of the disappearance of these resonances. Especially relevant to the present work are the analyses by Wynne [28] and by Elk, Lambropoulos, and Tang [29]. Wynne [28] extended these ideas to an atomic system similar in structure to ours, involving a transition which is both one-photon and three-photon allowed. By including a variety of optical interactions parametrically (a macroscopic polarization at the three-photon frequency corresponding to linear absorption and third-harmonic generation, and a macroscopic polarization at the fundamental frequency corresponding to four-wave difference frequency generation and three-photon absorption) Wynne showed that the field amplitudes and phases are stabilized, or locked to each other, at values at which there is precise destructive interference of the transition amplitude for excitation to the upper state. Elk *et al.* [29] later presented an improved analysis of this same $\omega - 3\omega$ interference, using an approach based on the Maxwell-Bloch equations. They arrived at the same conclusion, i.e., that the relative field amplitudes and phases automatically approach the condition of destructive interference. They also showed quantitatively the role of noninterfering channels of similar processes, derived a quantitative condition for the density at which destructive interference occurs, and outlined how to extend the analysis to the case of focused Gaussian beams.

We examine these effects at high densities by observations of the interference between the transition moments for a dipole-allowed transition in atomic mercury driven concurrently by a one-photon and a three-photon interaction. As the mercury density is increased, the medium couples the two

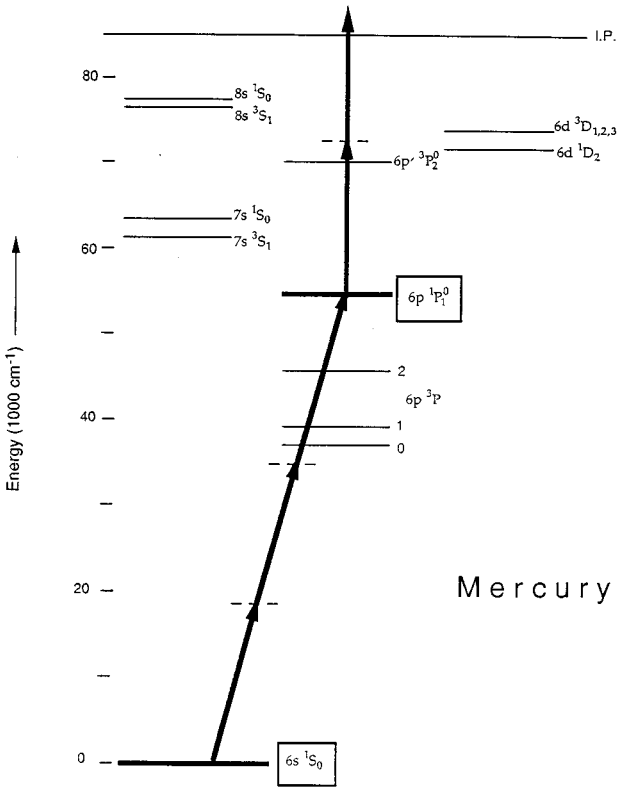

FIG. 1. Energy level diagram of mercury. The pulsed dye laser is tuned slightly to the blue of the resonance frequency of the three-photon $6s\ ^1S_0 \rightarrow 6p\ ^1P_1^o$ transition. We observe the resonantly enhanced multiphoton ionization signal under the condition of increasing density of the mercury vapor.

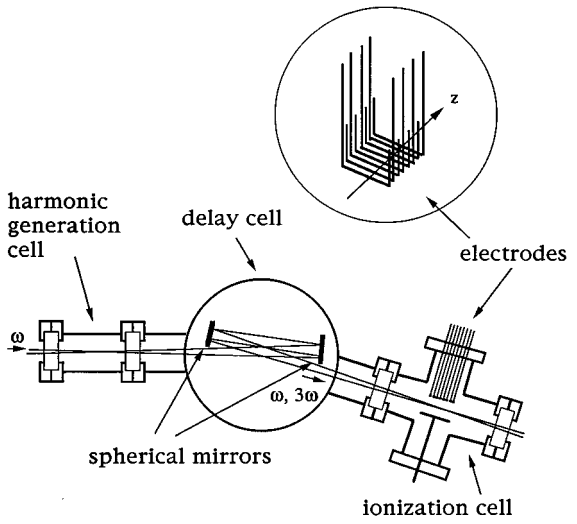

FIG. 2. Experimental cell used for the interference measurements. The fundamental laser beam is focused into the harmonic generation cell containing a vapor of mercury atoms which generate the third-harmonic field component. The two beams diverge from this cell collinearly, are collimated, and refocused by two spherical mirrors in the delay cell to the center of the ionization cell where we collect the photoelectrons using a configuration of eight collection electrodes. A detail of the electrodes is shown in the inset. (**z** indicates the direction of propagation of the laser beam.)

coherent field components to each other, affecting their relative phase and amplitude. We are able to measure these propagation effects throughout the focal region by using a unique multielectrode photoelectron collector. Thus we can study spatial effects of these interactions in detail. Following, in Secs. II and III, we describe our experiment and discuss its results. In Sec. IV, we apply the theory of Elk *et al.* [29], extending them somewhat to examine intermediate densities, and compare the results of this analysis to those of our experiment.

II. EXPERIMENT

The experiment is carried out using the system used for some of our prior observations of the interference [30], in which we measured diffractional phase shifts of a focused Gaussian beam using three-photon resonant, five-photon ionization of atomic mercury when driven concurrently by a two-color laser field. A homemade Littman-style short-cavity dye laser (Rhodamine 6G dye) and a two-stage amplifier, each longitudinally pumped by the second harmonic of a *Q*-switched Nd:YAG laser, are used to produce a nearly TEM_{00} Gaussian beam at a wavelength of $\lambda = 554$ nm (6-mJ pulse energy, 15-nsec pulse duration). At this wavelength the laser is tuned near the $6s\ ^1S_0 \rightarrow 6p\ ^1P_1^o$ three-photon transition. (See Fig. 1.) This beam is focused into the first cell (harmonic generation cell) of a three cell series, shown in Fig. 2, using a 20-cm focal-length lens. Coherent ultraviolet radiation at 185 nm is generated via a resonantly enhanced third harmonic generation process in the vapor of atomic mercury in this cell. As is critical for the observation of the interference, this third-harmonic radiation has a well-determined phase with respect to that of the laser fundamental. The visible and ultraviolet beams are collimated and refocused into the third cell (ionization cell) of the series using a pair of spherical mirrors (focal length = 37.5 cm) with a uv-enhanced aluminum coating. The angle of incidence of the laser beams on these spherical mirrors is kept small ($<3°$) in order to minimize astigmatic aberrations. The third cell also contains mercury vapor. The densities of mercury in the first and third cells are independently controllable by varying the cell temperatures. The second cell (delay cell) is used to vary the relative phase between the two field components. By varying the density of argon gas in this chamber, the phases of the visible and uv beams undergo a shift of magnitude $\phi_{vis} = 2\pi l \Delta\rho n^{554}/\lambda$ and $\phi_{uv} = 6\pi l \Delta\rho n^{185}/\lambda$, respectively, where l is the path length in the delay cell, $\Delta\rho$ is the change in density (in amagats), and n^{554} and n^{185} are the refractive indices of argon gas at STP conditions at 554 nm and 185 nm, respectively. A variation of $\Delta\phi = \phi_{uv} - 3\phi_{vis} = 2\pi$ results in a complete cycle in the modulation of the resonantly enhanced photoionization signal produced in the third cell.

The focal region in the ionization cell is approximately centered between a ground plane and a set of eight biased (+300 V) collection electrodes. Each electrode is constructed from a 1.27-mm-diam stainless-steel rod. They are aligned transverse to the direction of propagation of the laser beam, side by side, in a plane parallel to the ground plane with a center-to-center spacing of 1.65 mm. Each electrode collects the photoelectrons generated in the region directly

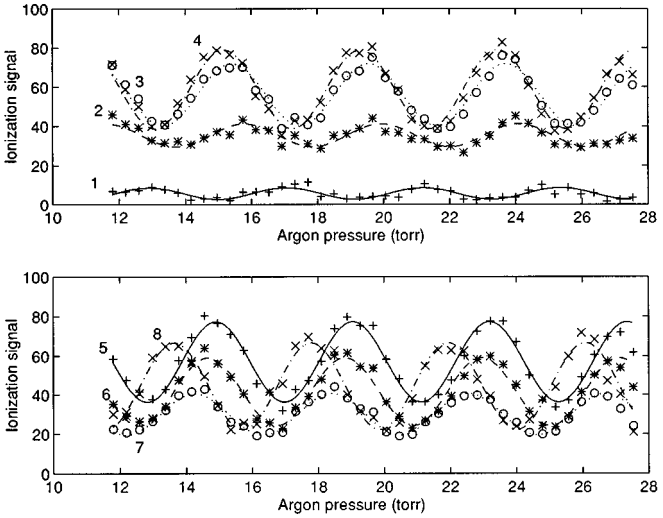

FIG. 3. Ionization signal as a function of argon gas pressure in the delay chamber for each of the eight electrodes. Electrodes are numbered 1–8, with 1 indicating the first electrode positioned before the focus and 8 the last electrode positioned after the focus.

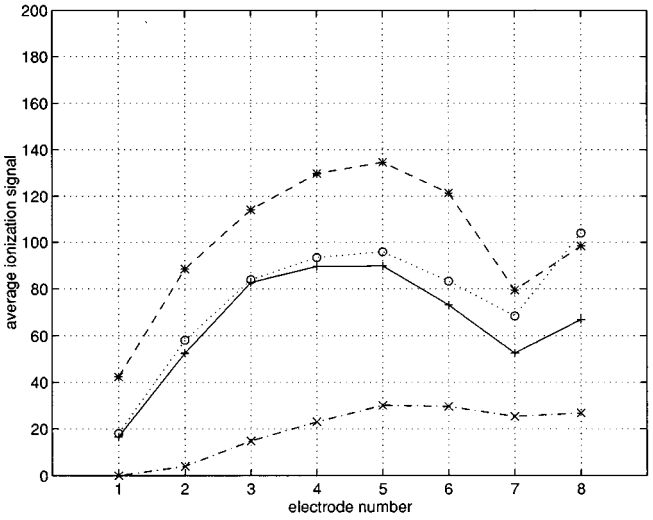

FIG. 4. Average ionization signal collected by each of the eight electrodes for four different densities of the mercury vapor in the ionization cell. ρ_3 is 1.0(+), 2.0(∗), 4.5(○), or 9.0(×) $\times 10^{14}$ cm^{-3}. The density in the harmonic generation cell is 30×10^{14} cm^{-3} for each curve.

between it and the ground plane. (The spatial resolution of the detector is approximately determined by the spacing between the electrodes, with a smaller contribution from the trajectory of the free electrons in the collection field.) The total charge detected by each of the electrodes for each laser pulse is determined concurrently by an eight-channel gated integrator, and recorded using a laboratory personal computer. In this way we are able to measure the number of photoelectrons generated in the laser beam at varying axial distances from the laser focus.

The laser cavity is short (about 5 cm) so that laser oscillation is limited to one to three laser modes on any given shot. Since the Q-switched Nd:YAG laser used to pump the dye laser operates on multiple longitudinal modes, there are shot-to-shot variations of the longitudinal mode structure of the dye laser. We observe no deleterious effects for this system attributable to this poor longitudinal mode quality. We monitor the power of each pulse of the dye laser, and collect data only for those pulses whose energy falls within a $\pm 7\%$ window. The beam is somewhat elliptical, with calculated beam radii of 20 μm and 34 μm at the focus of the beam in the ionization cell. The peak intensity of the laser fundamental is thus about 4×10^{10} W cm^{-2}. The confocal parameters for these beam radii are 0.45 cm and 1.31 cm, respectively. The peak integrated signal which we detect corresponds to the collection of about 5×10^5 electrons. At our vapor density and focal size, this corresponds to a maximum ionization probability of about 0.2%. In the following section, we discuss the experimental results obtained with the system discussed above.

III. RESULTS

A typical data set is shown in Fig. 3, where we have plotted the ionization signal as a function of the argon pressure in the delay cell for each of the eight collection electrodes. Each data point represents the average of the ionization signal over 60–80 laser shots, and is seen to vary sinusoidally with the argon pressure with a period of $\sim$ 4 Torr. This is in accord with the path length in the argon chamber (delay chamber), $l=75$ cm, and with published data for the dispersion in the refractive index of argon [31]. The phase shift of the signal from one electrode to the next due to the phase variation of a focused Gaussian beam can be observed in the figure. (The peak of the sinusoidal variation shifts consistently to the left from one electrode signal to the next.) By fitting a sinusoidal curve to each data set, we determine the relative phase shift, the amplitude, and the average value of each electrode signal.

In Fig. 4, we show the average ionization signal for each electrode for four different values of the mercury density in the third cell. Data are shown for a first-cell mercury density of $\rho_1=30\times 10^{14}$ cm^{-3}. Two observations are quite striking. First, the total ionization signal, corresponding to the sum of each of the individual electrode signals, is seen to first increase, reach a maximum at $\rho_3=2.0\times 10^{14}$ cm^{-3}, and then decrease with increasing density, ρ_3 . This is consistent with observations over the past 18 years in which the ionization signal was seen to disappear at high densities due to interfering pathways of excitation [15–18]. The second feature of these observations is that the distribution of the ionization appears to be shifting with increasing density. For low densities ($\rho_3=1.0\times 10^{14}$ cm^{-3}) the signal peaks near the center of the chamber, between electrodes 4 and 5. Note that electrodes 1 and 8, since they are at the end of the array, collect electrons from a larger volume of the mercury cell than do electrodes 2 through 7. Thus their signals are potentially enhanced relative to the interior electrodes. As the density in the third cell increases, the distribution shifts toward higher electrode number, i.e., toward the exit end of the cell. For $\rho_3=9.0\times 10^{14}$ cm^{-3} the peak of the distribution is shifted nearly to electrode 6.

We have also examined the average ionization rate for

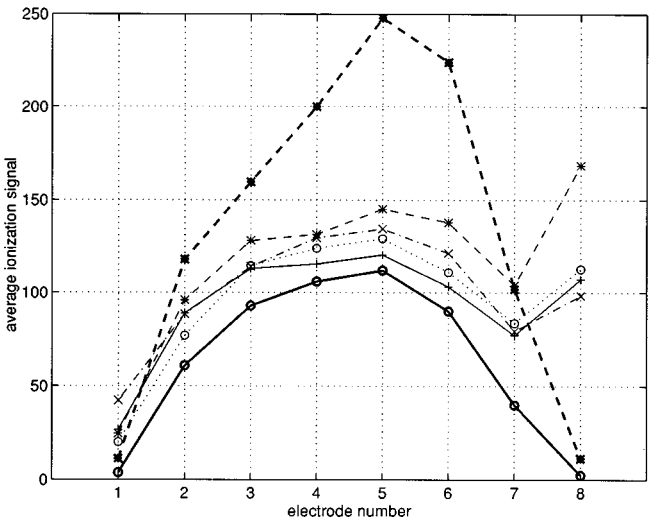

FIG. 5. Average ionization signal collected by each of the eight electrodes for six different densities of the mercury vapor in the harmonic generation cell. ρ_1 is 1.0(**o**), 2.0(**x**), 4.5(+), 9.0(∗), 14(○), and 30(×) $\times 10^{14}$ cm^{-3}. The density in the ionization cell is 2.0×10^{14} cm^{-3} for each curve.

each electrode as the intensity of the third-harmonic beam generated in the first cell is increased. This is shown in Fig. 5. The third-harmonic intensity increases with increasing density of the mercury vapor in the first cell, ρ_1 [18]. The distribution of the ionization signal is narrow for low ρ_1, and increases for larger ρ_1. For each data set in Fig. 5, the density in the third cell is $\rho_3 = 2.0\times 10^{14}$ cm^{-3}, a relatively low value at which propagation effects (wave coupling) are minimal. This broadening of the distribution is likely due to the intensity dependence of the one-photon process vs that of the three-photon process. With our multielectrode configuration, measurements of the spatial variation of the signal near the focus are, at low densities, equivalent to measurements of the intensity dependence. When ρ_1 is kept low, little third harmonic is generated in the first cell, and ionization in the third cell is predominantly due to the three-photon resonance of the laser fundamental with the $6s \rightarrow 6p$ resonance. The intensity dependence of this process (I^3 in the absence of saturation effects or population transfer) leads to ionization peaking in a region of dimension smaller than b, the confocal parameter of the focused beam. As the density of the first cell is increased, an increased intensity of third harmonic results, so that the linear interaction of this light with the atomic resonance becomes important, and ionization is strong over the entire range of length b centered about the focal spot. The confocal parameter b for the fundamental and harmonic beams is expected to be the same value [32].

The distributions of the average photoionization signal help us to understand something about the photionization rates out of the $6p\ ^1P_1^o$ level. As mentioned above, the measurements made using the multielectrode configuration amount to measurements of the intensity dependence of the interaction. Variation of the laser intensity through the focal region causes the ionization signal to peak in the center, and to fall off in either direction from there. We observe that in no case are we able to fit the data with an I^5 dependence. This dependence would result in a distribution which is peaked much more sharply at $z=0$. There are no data available on the photoionization cross sections for the $6p\ ^1P_1^o$ level, but from this intensity dependence it would appear that any atoms excited to the $6p\ ^1P_1^o$ are immediately photoionized. Since photoionization by the laser fundamental is only a second-order process, whereas excitation of the $6p\ ^1P_1^o$ is a third-order process, this assertion can be at least partially justified. We also expect that photoionization by the laser fundamental dominates over photoionization by the harmonic field. This expectation is justified on the basis of relative intensities of the two components of the field, as well as on the proximity to the photoionization threshhold.

There is also an apparent shift of the center of the distribution of the average ionization signal. This is possibly due in part to dispersion of the fused silica windows between the cells. We estimate that the windows (there are two between the focus in the first cell and the focus in the third cell, each of thickness 1/8 in., or 3.175 mm) will shift the location of the focus of the harmonic by about 1/3 mm with respect to that of the fundamental.

In Fig. 6 we show the dependence of the depth of modulation of the ionization signal collected by each electrode for four values of vapor density in the third cell. The depth of modulation is defined as the amplitude of the sinusoidal variation of the ionization signal divided by the average value. Data are shown for two different values of harmonic intensity input from the first cell. In both cases, the increasing role of locally generated harmonic with increasing ρ_3 can be seen. The depth of modulation starts very strongly at electrode 1, before the focus, where there has been no chance of local effects modifying the relative phase or amplitude of the harmonic field. As the beams propagate through the focal region, the amplitudes and phases tend to lock via the nonlinear coupling mechanism, resulting in a decreased amplitude of modulation as the beams emerge from the focal region (electrode 8). Phase and amplitude locking is very weak for low values of ρ_3, but quite evident for $\rho_3 = 4.5$ or 9.0×10^{14} cm^{-3}. It is interesting to note that, although the amplitude of the modulation is significantly suppressed for these high values of ρ_3, the average ionization rate is also suppressed (as shown in Fig. 4), so that the depth of modulation shown in Fig. 6 is only decreased by a factor of $\sim 1/2$ from the low ρ_3 value.

Finally, we show in Fig. 7 the ionization signal for each of the eight electrodes as a function of argon gas pressure (i.e., relative phase of the input field components) for two different values of ρ_3. For the left half of the plot, $\rho_3 = 2.0\times 10^{14}$ cm^{-3}, a relatively low value, while for the right half $\rho_3 = 9.0\times 10^{14}$ cm^{-3}, a large value. All the features discussed above, i.e., suppression of the average rate of ionization and of the amplitude of the modulation, can be seen here.

IV. THEORY

A recent theoretical report by Elk, Lambropoulos, and Tang [29] appeared in which they considered a very similar problem as we have presented here. While they were motivated by experiments which had been carried out in xenon [33], the system was similar to that of our mercury experi-

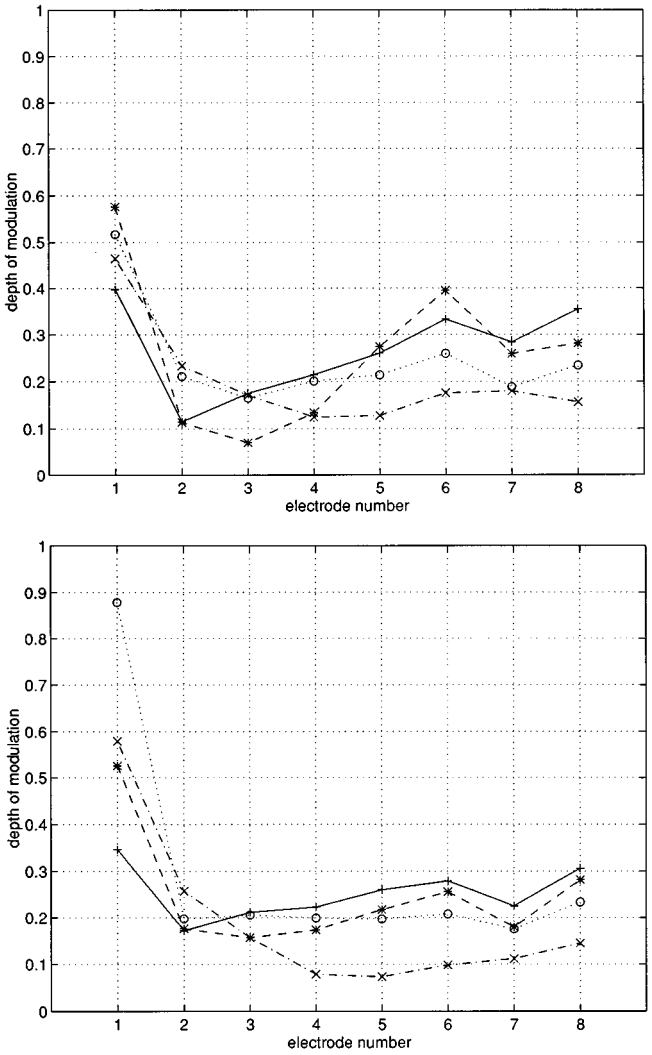

FIG. 6. The depth of modulation of the ionization signal collected by each of the eight electrodes for four different densities of the mercury vapor in the ionization cell. ρ_3 is 1.0(+), 2.0(∗), 4.5(○), or 9.0(×) $\times 10^{14}$ cm^{-3}. The density in the generation cell is 9.0×10^{14} cm^{-3} for each curve in (a), and 14×10^{14} cm^{-3} for each curve in (b).

ment in that the fundamental laser was near three-photon resonance with a dipole-allowed transition, and the xenon was photoionized by the absorption of two additional fundamental photons. Their work was based upon a Maxwell-Bloch formalism, and they considered the atomic vapor to be composed of two-level absorbers which interacted with a two-frequency optical field consisting of a laser fundamental and its third harmonic, of amplitude $\mathscr{E}_{vis}(z)$ and $\mathscr{E}_{uv}(z)$, respectively. The field component $\mathscr{E}_{vis}(z)$ is that of an undepleted focused Gaussian beam,

$$\mathscr{E}_{vis}(z)=\mathscr{E}_{vis,0}\frac{\exp(-ikz)\exp\left(-\dfrac{k(x^2+y^2)}{b(1-i\xi)}\right)}{1-i\xi}, \qquad (1)$$

where $\mathscr{E}_{vis,0}$ is the on-axis field amplitude at the focus, $k=2\pi/\lambda=n\omega/c$ is the wave number of the fundamental (in-

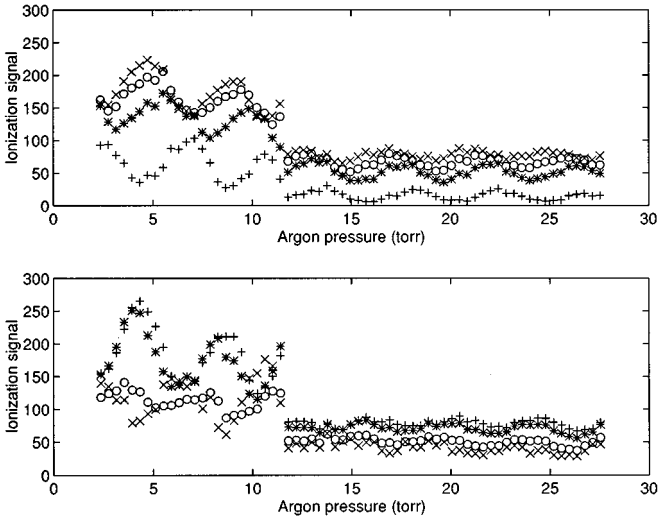

FIG. 7. Ionization signal as a function of argon gas pressure in the delay chamber for each of the eight electrodes. Data on the left half (pressure $<$ 11.5 torr) correspond to a density of $\rho_3 = 2.0 \times 10^{14}$ cm^{-3}, while for data on the right half (pressure $>$ 11.5 torr) the density has been increased to 9.0×10^{14} cm^{-3}. The curves in the upper panel are for electrodes 1(+), 2(∗), 3(○), and 4(×), while 5(+), 6(∗), 7(○), and 8(×) are shown below.

cluding refractive index phase variations corresponding to all transitions in the mercury *except* the $6s\ ^1S_0\rightarrow 6p\ ^1P_1^o$ transition) [34], $\xi=2z/b$ is the normalized dimension in the direction of propagation of the beam, b is the confocal parameter of the beam, and ω is the frequency of the laser. The amplitude of the harmonic field in their work was zero at the input, but this is easily adjusted as an initial condition in the integration of the wave equation. An ac Stark shift of the transition resonant frequency, ω_{21}, is incorporated by including a term linearly proportional to the laser intensity, $\delta\omega_{21}$, in the expression for the detuning of the laser from resonance,

$$\Delta=\omega_{21}-3\omega+\delta\omega_{21}. \qquad (2)$$

They invoke the adiabatic approximation in their solution of the optical Bloch equations, valid when the rate of variation of the Bloch vector components is slow compared to the ionization rate from the $6p$ level, γ, the Rabi precession rate, Ω, the spontaneous emission decay rate, $1/\tau$, or other rates characterizing the interaction. As the rate of photoionization appears to be so rapid in our experiment, we believe that this approximation is likely valid in our case, as well. In this limit, Elk *et al.* show that the off-diagonal element of the Bloch vector is of the form

$$\sigma_{12}^{(3)}=\frac{\mathscr{E}_{uv}(z)\mu_{12}+\mathscr{E}_{vis}^3(z)\exp(i\Delta k^{NR}z)\mu_{12}^{(3)}}{\hbar(\Delta+i\Gamma/2)}n(z), \qquad (3)$$

where μ_{12} is the transition dipole moment, $\Delta k^{NR}\equiv k^{uv}-3k$ is the wave number mismatch (including only nonresonant contributions to the refractive index), $\mu_{12}^{(3)}$ is the generalized three-photon dipole moment,

$$\mu_{12}^{(3)}=\sum_{m,l}\frac{\mu_{1m}\mu_{ml}\mu_{l2}}{(\omega-\omega_{m1})(2\omega-\omega_{l1})}, \tag{4}$$

Γ is the decay rate of the coherence of the interaction (including the transverse lifetime of the transition, T_2, the laser bandwidth, and the ionization rate), and $n(z)=\sigma_{11}-\sigma_{22}$ is the slowly varying population difference between the $6s$ and $6p$ levels. The macroscopic polarization related to this element is the source term in the wave equation, and Elk *et al.* show that at large densities the third-harmonic amplitude and phase tend to a value that strongly suppresses the resonantly enhanced multiphoton ionization rate. Following their approach, and assuming that the harmonic beam also has a transverse Gaussian profile [expressed in a form similar to Eq. (1)], we determine that the rate of change of the harmonic field amplitude is governed by

$$\frac{\partial}{\partial z}\mathscr{E}_{uv,0}(z)=-ia\left[\frac{\chi^{(3)}\exp(i\Delta k^{NR}z)\mathscr{E}_{vis,0}^{3}(z)}{(1-i\xi)^2}+\chi^{R(1)}\mathscr{E}_{uv,0}(z)\right], \tag{5}$$

where

$$a=\frac{2\pi\omega_3}{n_3 c}, \tag{6}$$

$$\chi^{(3)}=\chi^{NR(3)}+\frac{\rho\mu_{12}^{(3)}\mu_{21}n(z)}{\hbar(\Delta+i\Gamma/2)}, \tag{7}$$

and

$$\chi^{R(1)}=\frac{\rho|\mu_{12}|^2 n(z)}{\hbar(\Delta+i\Gamma/2)}. \tag{8}$$

In these expressions n_3 and $\chi^{NR(3)}$ are the contributions to the refractive index at 185 nm and to the third-order hyperpolarizability for third-harmonic generation for all atomic transitions except the $6s\rightarrow 6p$ transition. With this we derive an ionization rate, per atom, of

$$(\gamma_1+\gamma_3)\sigma_{22}=\frac{\Gamma n(z)}{1+1/[\tau(\gamma_1+\gamma_3)]}\times\frac{|\mathscr{E}_{uv}(z)\mu_{12}+\mathscr{E}_{vis}^{3}(z)\exp(i\Delta k^{NR}z)\mu_{12}^{(3)}|^2}{\hbar[\Delta^2+(\Gamma/2)^2]}. \tag{9}$$

Numerically integrating Eq. (5) to determine the variation in $\mathscr{E}_{uv,0}(z)$, and then computing the ionization rate using Eq. (9), we are able to calculate the average value of the ionization rate, as well as the magnitude of the modulation. These are shown as a function of z in Fig. 8 for densities $\rho_3=7.5$, 15, and 30×10^{14} cm^{-3}. The four curves shown for each density correspond to the photoionization rate for four different phases of the input harmonic field (projected to the focus) $\mathscr{E}_{uv,0}(-\infty)$. The phase difference of the input field for one curve to the next is 90°. Other parameters used in our computations are peak intensity of the fundamental beam at the focus $=5\times10^{10}$ W cm^{-2}, $\mu_{12}=1.31\times10^{-29}$ C m,

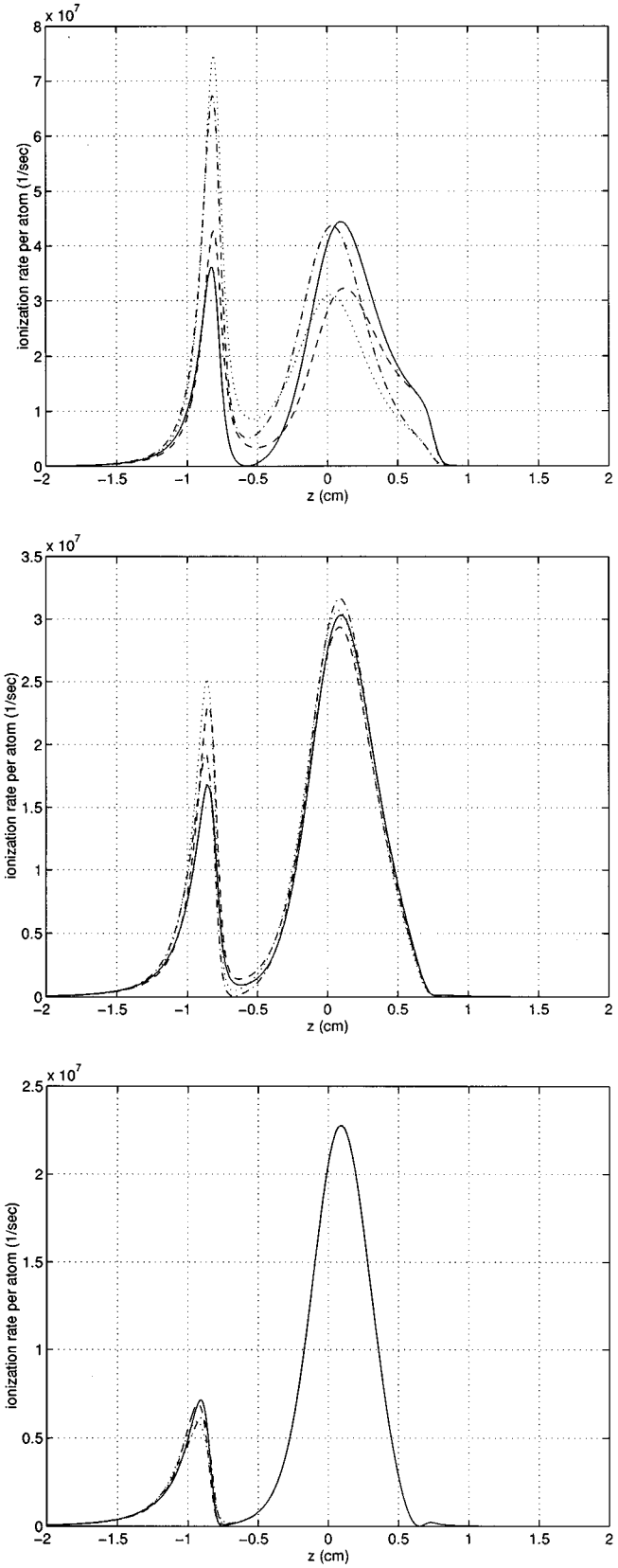

FIG. 8. Calculated ionization rate vs position. The focus of the laser beam is located at $z=0$. The four curves in each panel correspond to four different phases of the input field. The density of the mercury atoms in the ionization cell is ρ_3 = 7.5, 15, and 30 $\times10^{14}$ cm^{-3} for (a), (b), and (c), respectively.

$\mu_{12}^{(3)}=2\times10^{-50}$ C^3 m^3 J^{-2}, $\omega_{21}-3\omega=-1.8\times10^{13}$ rad/sec, $n(z)=1$ everywhere, Stark shift $=0.14$ rad/sec/(W cm^{-2}) [35,36], $T_2=2.6$ nsec, $\tau=1.3$ nsec [37,38], laser bandwidth $=5$ GHz, cross section for two-photon ionization of the $6p\ ^1P_1$ level by the laser fundamental $=5\times10^{-45}$ cm^4 s, and cross section for one-photon ionization of the $6p\ ^1P_1$ level by the laser harmonic $=1\times10^{-16}$ cm^2. When examining these figures, keep in mind that the intensity of the laser has a Gaussian profile, but the plots show only the photoionization rate on the axis of the laser beam. This is important because of the large ac Stark shift for this interaction, and the role it plays in the photoionization process. The photoionization shows two dominant peaks, one at about $z=-0.8$ cm and one at the focus, $z=0$. The first peak occurs at the point where the ac Stark shift moves the $6s\rightarrow6p$ transition into exact resonance with the laser frequency. The magnitude of this peak depends strongly (approximately linearly) on the input intensity of the uv field component. We do not expect, of course, that this peak would be observable in an experiment since it only occurs at this position on the laser axis. Off the laser axis the peak will occur closer to the focus.

The peak at the focus corresponds to the position at which the intensity of the laser fundamental reaches its peak value. The Stark shift has moved the atomic transition frequency well beyond resonance with the laser at this point, so this peak is dominated by nonresonant five-photon ionization.

Both peaks show modulation as the phase of the input harmonic is varied, but the modulation is clearly stronger for the first peak than for the second. This is a symptom of the locking of the relative phase and magnitude of the beams via their interaction with the mercury vapor as they propagate towards the focus of the beam. For $\rho_3=30\times10^{14}$ cm^{-3}, there is still significant ionization signal, yet no visible modulation of the ionization signal. The waves are strongly coupled via their interaction with the absorbing medium, thus the absence of modulation, but at these densities they are coupled to values which do not lead to complete destructive interference of the resonance. Our computations indicate that the rapid variation of the field amplitudes through the focal region makes it difficult for the nonlinear medium to efficiently couple the fundamental and harmonic waves, so that suppression of the photoionization signal is not complete. The modulation necessary for control, however, is significantly reduced at increased densities.

There is a great deal of room for improvement of these model calculations. The two most significant improvements are (i) to include the effects of the transverse Gaussian profile of the beam, and (ii) to improve the parameters used for the three-photon dipole moment of mercury. The wave equation includes a transverse differentiation which we circumvented by assuming that the harmonic field will have a transverse Gaussian profile as well. This assumption is valid in the absence of Stark shifts, but poorly deficient in the present case. We hope that this report will stimulate sufficient interest that proper treatment of this problem will be undertaken. Additionally, the parameters which we have chosen to use for our calculations have varying degrees of legitimacy. The oscillator strength and lifetime, τ, for the $6s\ ^1S_0\rightarrow6p\ ^1P_1^o$ transition have been measured by several groups [37,38], so we have confidence in the value of μ_{12} employed. Similarly, the Stark shift coefficient [35,36], resulting from the near resonance of the laser fundamental frequency with the $6p\ ^1P_1^o\rightarrow6d\ ^1D_2$ transition, is reasonably well measured. We have used $T_2=2\tau$, since at these densities collisional effects should be minimal. Little is known of $\mu_{12}^{(3)}$ or either of the two photoionization cross sections, however. We estimated a value for $\mu_{12}^{(3)}$ using Eq. (4) with $m=2$, $l=1$, and doubling the result to very roughly approximate the contribution due to all other states m,l. For the rate of photoionization out of the $6p\ ^1P_1^o$ level, we expect that, at our intensities, the two-photon ionization rate is somewhere around 10^{14} s^{-1}, as discussed in Sec. III. We chose the two-photon cross section to yield this value. The cross section for linear photoionization of the $6p\ ^1P_1$ by the laser harmonic was not critical. Clearly, improvements of these parameters will help us to understand our measurements more fully.

V. CONCLUSION

In this paper we have reported our experimental measurements of two-color coherent control of resonantly enhanced photoionization in atomic mercury. We have observed the dependence of this interference on the density of the mercury vapor at an array of positions throughout the focal region of the exciting laser beam. In all cases modulation of the photoionization signal is very strong before the laser beams reach the focus. After the focus, we observe that this phase-controlled modulation, while decreased in amplitude, is still visible, even at densities at which the average photoionization signal is significantly suppressed by interference involving the locally generated harmonic field. A simplified numerical axial integration of the optical Bloch equations shows (i) that the ac Stark shift plays an important role in these interactions, (ii) that suppression of the resonantly enhanced ionization signal at elevated densities is not as complete for focused beams as it is for plane waves due to the rapid variation of the field amplitudes and phases in the focal region, and (iii) that the phase and amplitude of the third-harmonic field component are relatively insensitive to input conditions at densities which lead to only partial suppression of the resonance. This third conclusion resulting from the numerical analysis is not supported by our experimental observations, perhaps because of the presence of off-axis ionization not included in the numerical studies. More rigorous techniques would be very helpful in a more complete interpretation of our results.

ACKNOWLEDGMENTS

Partial funding of this work by the National Science Foundation, Grant No. 9017224-PHY, and the Office of Naval Research, Grant No. N00014-92-J-1882, is gratefully acknowledged.

[1]

[1] Paul Brumer and Moshe Shapiro, Acc. Chem. Res. **22**, 407 (1989); M. Shapiro, J.W. Hepburn, and P. Brumer, Chem. Phys. Lett. **149**, 451 (1988); C.K. Chan, P. Brumer, and M. Shapiro, J. Chem. Phys. **94**, 2688 (1992).
[2] Ce Chen, Yi-Yian Yin, and D.S. Elliott, Phys. Rev. Lett. **64**, 507 (1990).
[3] S.M. Park, S.-P. Lu, and R.J. Gordon, J. Chem. Phys. **94**, 8622 (1992).
[4] H.G. Muller, P.H. Bucksbaum, D.W. Schumacher, and A. Zavriyev, J. Phys. B **23**, 2761 (1990); D.W. Schumacher, F. Weihe, H.G. Muller, and P.H. Bucksbaum, Phys. Rev. Lett. **73**, 1344 (1994).
[5] Yi-Yian Yin, Ce Chen, D.S. Elliott, and A.V. Smith, Phys. Rev. Lett. **69**, 2353 (1992).
[6] N.B. Baranova, I.M. Beterov, B. Ya. Zel'dovich, I.I. Ryabtsev, A.N. Chudinov, and A.A. Shul'ginov, Pis'ma Zh. Éksp. Teor. Fiz. **55**, 431 (1992) [JETP Lett. **55**, 439 (1992)].
[7] Yi-Yian Yin, D.S. Elliott, R. Shehadeh, and E.R. Grant, Chem. Phys. Lett. **241**, 591 (1995).
[8] V.D. Kleinman, L. Zhu, X. Li, and R.J. Gordon, J. Chem Phys. **102**, 5863 (1995).
[9] B. Sheehy, B. Walker, and L.F. DiMauro, Phys. Rev. Lett. **74**, 4799 (1995).
[10] N.B. Baranova, A.N. Chudinov, and B. Ya. Zel'dovich, Opt. Commun. **79**, 116 (1990); N.B. Baranova, A.N. Chudinov, A.A. Shul'ginov, and B. Ya. Zel'dovich, Opt. Lett. **16**, 1346 (1991).
[11] Vince Dominic and Jack Feinberg, Phys. Rev. Lett. **71**, 3446 (1993); J. Opt. Soc. Am. B **11**, 2016 (1994).
[12] E. Dupont, P.B. Corkum, H.C. Liu, M. Buchanan, and Z.R. Wasilewski, Phys. Rev. Lett. **74**, 3596 (1995).
[13] L. Zhu, V. Kleiman, X. Li, S.P. Lu, K. Trentelman, and R.J. Gordon, Science **270**, 77 (1995).
[14] Takashi Nakajima and P. Lambropoulos, Phys. Rev. Lett. **70**, 1081 (1993).
[15] K. Aron and P.M. Johnson, J. Chem. Phys. **67**, 5099 (1977).
[16] F.H.M. Faisal, R. Wallenstein, and H. Zacharias, Phys. Rev. Lett. **39**, 1138 (1977).
[17] R.N. Compton, J.C. Miller, and A.E. Carter, Chem. Phys. Lett. **71**, 87 (1980); J.C. Miller, R.N. Compton, M.G. Payne, and W.R. Garrett, Phys. Rev. Lett. **45**, 114 (1980); J.C. Miller and R.N. Compton, Phys. Rev. A **25**, 2056 (1982); M.G. Payne, W.R. Garrett, and W.R. Ferrell, *ibid.* **34**, 1143 (1986); W.R. Garrett, W.R. Ferrell, M.G. Payne, and J.C. Miller, *ibid.* **34**, 1165 (1986).
[18] D. Normand, J. Morellec, and J. Reif, J. Phys. B **16**, L227 (1983).
[19] É.A. Manykin and A.M. Afanas'ev, Zh. Eksp. Teor. Phys. **48**, 931 (1965); **52**, 1246 (1967) [Sov. Phys. JETP **21**, 619 (1965)]; **25**, 828 (1967).
[20] G.L. Gurevich and Yu.G. Khronopulo, Zh. Eksp. Teor. Phys. **51**, 1499 (1966) [Sov. Phys. JETP **24**, 1012 (1967)].
[21] J.H. Glownia and R.K. Sander, Appl. Phys. Lett. **40**, 648 (1982); Phys. Rev. Lett. **49**, 21 (1982).
[22] Y.I. Geller and A.V. Shvabouskas, Opt. Spektrosk. **53**, 385 (1982) [Opt. Spectrosc. (U.S.S.R.) **53**, 227 (1982)].
[23] S. A. Bakhramov, I. Kirin, P.K. Khabibullaev, and N.S. Shaabdurakhmanova, Kvant. Elektron. (Moscow) **9**, 2386 (1982) [Sov. J. Quantum Electron. **12**, 1557 (1982)].
[24] M.S. Malcuit, D.J. Gauthier, and R.W. Boyd, Phys. Rev. Lett. **55**, 1086 (1985); R.W. Boyd, M.S. Malcuit, D.J. Gauthier, and K. Rzazewski, Phys. Rev. A **35**, 1648 (1987).
[25] M.G. Payne, W.R. Garrett, and H.C. Baker, Chem. Phys. Lett. **75**, 468 (1980); M.G. Payne and W.R. Garrett, Phys. Rev. A **26**, 356 (1982); **28**, 3409 (1983).
[26] D.J. Jackson and J.J. Wynne, Phys. Rev. Lett. **49**, 543 (1982); D.J. Jackson, J.J. Wynne, and P.H. Kes, Phys. Rev. A **28**, 781 (1983).
[27] M. Poirier, Phys. Rev. A **27**, 934 (1983).
[28] James J. Wynne, *Multiphoton Processes*, Proceedings of the Fourth International Conference on Multiphoton Processes, Boulder, 1987, edited by S.J. Smith and P.L. Knight (Cambridge University Press, Cambridge, 1987), p. 318.
[29] Morten Elk, P. Lambropoulos, and X. Tang, Phys. Rev. A **46**, 465 (1992).
[30] Ce Chen and D.S. Elliott, Phys. Rev. Lett. **65**, 1737 (1990).
[31] C. Cuthbertson and M. Cuthbertson, Proc. R. Soc. London **84**, 13 (1910); M. Rusch, Ann. Phys. (Leipzig) **70**, 373 (1923); B. Quarder, *ibid.* **70**, 255 (1924).
[32] J.F. Ward and G.H.C. New, Phys. Rev. **185**, 57 (1969).
[33] C. Charalambidis, X. Xing, J. Petrakis, and C. Fotakis, Phys. Rev. A **29**, 1922 (1991).
[34] Rita Mahon and Frank Tomkins, IEEE J. Quantum Electron. **18**, 913 (1982).
[35] Arlee V. Smith, Opt. Lett. **10**, 341 (1985).
[36] M. Poirier, J. Reif, D. Normand, and J. Morellec, J. Phys. B **17**, 4135 (1984).
[37] Allen Lurio, Phys. Rev. **140**, A1505 (1965).
[38] Ausma Skerbele and Edwin N. Lassettre, J. Chem. Phys. **52**, 2708 (1970).